Chapter 6: Adsorption and activation of nitric oxide (NO) and oxygen (O_2) on bare and supported M_n/ZSM-5[M=Au, Pd, Pt] (n=1-2) using ONIOM method

Abstract

Herein, in Chapter 6, we have investigated the adsorption and activation pattern of nitric oxide (NO) and oxygen (O_2) on bare and supported M_n/ZSM-5[M=Au, Pd, Pt] (n=1-2). In order to investigate the adsorption properties, we have employed density functional theory (DFT) with ONIOM2 (QM: MM) (wB97XD/LANL2DZ/6-31G(d,p):UFF) calculations. Adsorption analysis is an effective method for determining a catalyst's active sites and how reactants attach to them. An ideal or moderate contact between the reactants and the catalysts is required in order to activate the molecules, which in turn drive the reaction in the forward direction. Zeolite is an excellent host material, with high size and shape selectivity and well-defined holes and channels. Because of their relatively great thermal stability, they can carry out reactions in both gas and liquid phases under difficult conditions. Well-defined metal clusters on a support material, such as zeolites, act as a bridge between the traditional field of heterogeneous catalysis research and fundamental gas-phase investigations. In this study, the impact of support on the activation and adsorption energies of NO and O_2 was investigated. The findings show that the interactions between molecule-cluster and cluster-framework might cause an increase or decrease in adsorption energies of NO and O_2 when compared to gas-phase clusters.

Graphical Abstract

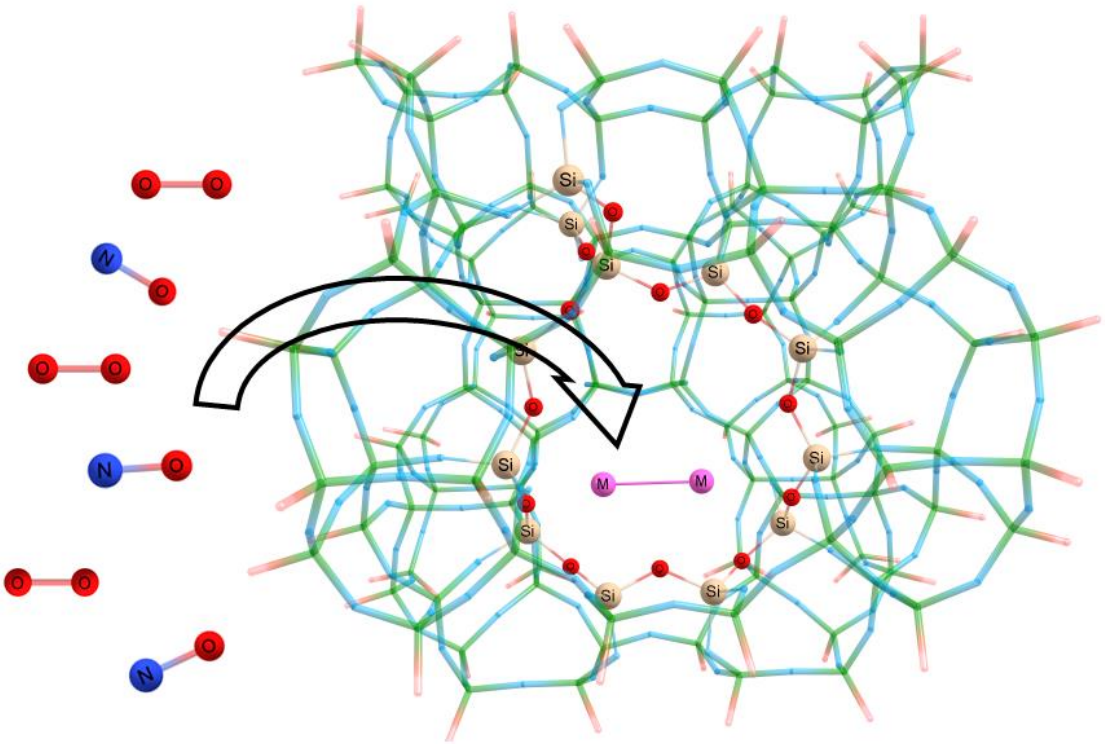

M=(Au, Pd & Pt)

6.1 Introduction

Nitrogen oxides (NO_x) are typical air pollutants responsible for stratospheric O_3 depletion [1], acid rain in the troposphere [2] and photochemical smog. The main sources for NO_x emissions comes from automobile exhausts and power plants [3]. Since, NO is an insoluble pollutant in flue gas [4], it is important to convert NO to NO_2 using strong oxidants and then reduce NO_2 to N_2 with the help of a reductant [5]. Subnanometric metal species consisting of single atoms and clusters, show unique and distinct properties from their nanoparticulate counterparts. However, the catalytic applications of subnanometric metal species is limited by their poor stability towards sintering at high temperature (>500 °C) under oxidative or reductive reaction conditions. Capturing the nanosized metal species inside the support's confined space is an effective method to stabilize them. In this regard, zeolites are an ideal option of support due to their large surface area, well-defined pore structure, along with excellent thermal stability. In numerous investigations, zeolites have been proven to be capable to stabilize metal nanoparticles (NPs) against thermal sintering by encasing them inside their micropores [6-9].

Various other materials, such as supported noble metals, coinage metal oxides and early transition metal oxides, have been studied [10-11] before zeolite catalysts. The most pertinent and helpful prior information comes from the development of oxide supported vanadia SCR systems, which were started in Japan in the early 1970s and are currently being used all over the world for stationary NO_x removal applications [10]. Due to the extensive experience with vanadia-based SCR catalysts in stationary applications, this catalyst system has actually been commercialized in Europe and has been considered for automotive applications for a long period [12]. However, because of concerns about vanadia waste from production processes, metal exchanged zeolites are presently being employed more commonly for vehicle NH_3-SCR applications.

Zeolites have undergone extensive investigation for their usage in catalytic processes such as selective catalytic reduction of nitrogen oxides [13, 14], biomass conversion [15], conversion of natural gas into value-added products [16], methanol-to-hydrocarbon conversion [17], etc. Gu *et al.* [18] examined NO adsorption as well as desorption on Pd/ZSM-5. Pd/ZSM-5 can act as passive NOx

adsorbers (PNAs) as it can store NOx at low temperatures and aid in mitigating cold start NOx emissions from diesel engines. Additionally, they investigated how temperature affected NO adsorption and put forth a mechanism for how NO adsorption and the formation of different surface intermediates occur. Mechanistic aspects of NO adsorption/desorption over Pd/SSZ-13 material were investigated using micro-reactor and operando FT-IR where NOx adsorption and desorption tests were carried out [19]. The experimental results show that even in the presence of exhaust species like propylene and CO, Pd/SSZ-13 is a reasonably effective NO storage material. Grybos *et al.* [20] used density-functional calculations with periodic boundary conditions to investigate NO adsorption on Pd_n (n=1-6) clusters supported on mordenite. After an extensive investigation of the cluster-support interactions and adsorption properties, it was found that cluster-support interactions cause a greater blueshift on NO-stretching modes than NO adsorbed on a free cluster. Density functional calculations were used to examine the effects of B and Ga's Al isomorphic substitution on the geometries, adsorption energies, and vibrational frequencies of NO and N_2O on a model for Au(I)/ZSM-5 catalysts [21]. It was discovered that isomorphous substitution changed the electronic properties of Au(I) in ZSM-5, which helped to promote NO adsorption. The adsorption and co-adsorption of NO SCR-HC (NO, C_3H_6 and O_2) on several zeolites (non-acidic NaY, acidic H-Beta and H-ZSM-5) modified with gold have been studied by Sobczak and colleagues [22]. They proposed that Au/H-Beta and Au/H-ZSM-5 zeolites, which have high Si/Al ratios, are the prominent catalysts for NO-SCR with propene.

Catalytic reactions often occur at catalyst's surfaces or interfaces, where gas reactants are adsorbed and transformed into products [23]. Adsorption analysis is the most effective method of determining a catalyst's active sites and how reactants attach to them. An optimal contact between the reactants and catalysts is required to activate the molecules, which aids the reaction. It is vital to evaluate the structure-activity correlations regarding the underlying gas sensing and catalytic capabilities for harmful gases on support systems. Therefore, it is imperative to examine the adsorption characteristics of NO and O_2 on precious metal M_n [M=Au, Pd, Pt] (n=1-2) supported on ZSM-5.

6.2 Computational Details

In order to optimize the electronic structures related to the adsorption of NO and O_2 on metal supported zeolites, we have implemented hybrid quantum mechanics/molecular mechanics (QM/MM) calculations utilizing ONIOM [24-25] method based on the Kohn-Sham density functional theory (DFT) calculations. The software we have used here is Gaussian 16 [26]. The system is composed of two parts: an exterior region called the molecular mechanical (MM) part and an active chemical region called the quantum mechanical (QM) part. ONIOM partitions a system into layers typically, high layer and low layer. High layer is treated with QM part while low layer is treated with MM part. More than two parts are also possible in ONIOM (QM:QM:MM). Generally, ONIOM energy is obtained via subtractive scheme. The interaction between QM and MM regions depend on the embedding scheme. There are two main embedding scheme; mechanical embedding and electronic embedding. In mechanical embedding, entire system is treated separately, but the interactions between layers are simplified. In electronic embedding, QM calculation includes polarization from the MM environment. The embedding used here for zeolite system is mechanical embedding.

Zeolite catalytic function can be studied at the nanoscale scale with the help of hybrid quantum mechanics/molecular mechanics approaches [25, 27-28]. A cluster model of $Si_{128}O_{219}H_{74}$, whose terminal oxygen atoms are saturated by H atoms, describes the ZSM-5 framework that we have employed in our work and is shown in Figure 6.1. We have selected a 10 member ring consisting of 10 oxygen atoms and 10 silicon atoms whose positions are relaxed. Two additional Si and O atoms connected to T12 site of the ring are also relaxed. The molecular mechanics portion utilizes the UFF force field [28, 29] due to its simplicity and lack of partial charges on the UFF atoms. It has also been indicated that UFF force field provides an appropriate description of the short-range van der Waals interactions. The wB97XD functional, which is based on the D2 Grimme model [30], has been used to account for the dispersion forces. According to recent studies, wB97XD [31, 32] functional can effectively describe zeolite systems. The ECP basis set LANL2DZ (Los Alamos National Laboratory 2 double ζ) [33, 34] has been utilized for Au, Pd, and Pt atoms, whereas the 6-31G (d, p) [35] basis set has been utilized for H, C, O, and Si atoms.

The stable adsorption intermediates are characterized in the frequency calculations by the absence of imaginary frequency. Adsorption energies of NO and O_2 on bare M_n (n=1-2) are calculated using equation (1) and (2) respectively while adsorption energies of NO and O_2 on M_n (n=1-2) supported on ZSM-5 are calculated using equation (3) and (4), respectively.

$$E_{ads\_NO} = E_{M\_NO} - E_M - E_{NO} \quad (1)$$

$$E_{ads\_O_2} = E_{M\_O_2} - E_M - E_{O_2} \quad (2)$$

$$E_{ads\_NO} = E_{M\_zeolite\_NO} - E_{M\_zeolite} - E_{NO} \quad (3)$$

$$E_{ads\_O_2} = E_{M\_zeolite\_O_2} - E_{M\_zeolite} - E_{O_2} \quad (4)$$

where E_{M_NO}, E_M, E_{NO} represents zero-point corrected energies of NO adsorbed on bare metal, bare metal and NO, respectively. $E_{M\_O_2}$ and E_{O_2} represents zero-point corrected energies of O_2 adsorbed on bare metal and O_2, respectively. $E_{M\_zeolite\_NO}$, $E_{M\_zeolite\_O_2}$ and $E_{M\_zeolite}$ represents zero-point corrected energies of NO adsorbed-on metal supported on zeolite, O_2 adsorbed on metal supported on zeolite and simple metal supported zeolite, respectively. Natural Bond orbital (NBO) study has also been performed to acquire a better understanding of the charge transfer [36].

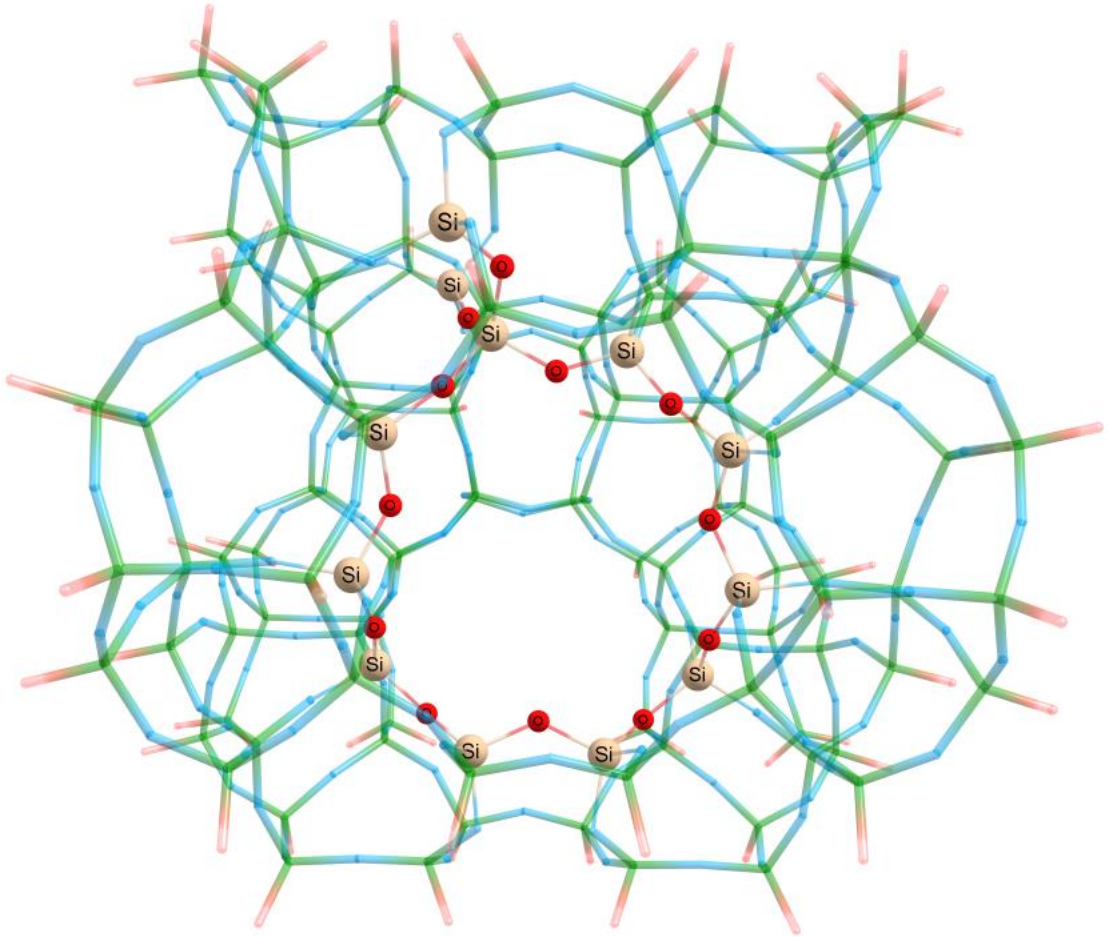

Figure 6.1: ZSM-5 unit where ball model represents QM region while thin stick model represents MM region. In MM region, green represents Si atom, blue represents O atom and pink represents H atom.

6.3 Results and Discussion

6.3.1 Cluster framework interaction energies

First of all, it is important to know the interaction between the clusters and the zeolite framework. Equation 5 defines the binding energy, which indicates the strength of the interaction between a neutral cluster and a completely siliceous ZSM-5 framework.

$$E_{bind}\,(M_n\,) = E_{Zeolite} + E_{M_n} - E_{M_n\_Zeolite} \qquad (5)$$

where $E_{Zeolite}$ represents energy of purely siliceous ZSM-5, E_{M_n} denotes energy of M element (M=Au, Pd and Pt) (n=1-2) and $E_{M_n\_Zeolite}$ represents energy of M_n system embedded on ZSM-5 framework.

Table 6.1: Binding energies of M_n (M=Au, Pd and Pt) (n=1-2) with purely siliceous (Al-free) ZSM-5 system.

Species	E_{bind} $(in\ kcal/mol)$
Au	-6.36
Au_2	15.70
Pd	-5.22
Pd_2	11.13
Pt	-2.92
Pt_2	48.88

From Table 6.1, it is evident that the formation of single atom catalyst in a purely siliceous ZSM-5 system is energetically unfavorable. Single atoms (M=Au, Pd, and Pt) will diffuse through the zeolite's channels rapidly, as indicated by negative binding energies towards ZSM-5. However, E_{bind} for each dimer system is highly positive, thus, indicating stability. Hence, the formation of dimer system for M=Au, Pd and Pt with purely siliceous ZSM-5 is energetically favorable.

The simplest way to "build" a cluster is to add to an already-existing cluster with M atom from the gas phase. The building energy of such process is given by-

$$E_{build}\,(M_n) = E_{M_n\_Zeolite} - E_{M_{n-1}\_Zeolite} - E_{M_1} \qquad (6)$$

where $E_{M_n\_Zeolite}$ and $E_{M_{n-1}\_Zeolite}$ are the energies of M element (M=Au, Pd and Pt) of sizes n and n-1 respectively. E_{M_1} represents energy of an isolated, single gas phase M atom (M=Au, Pd and Pt). The building energy is given in Table 6.2. From Table 6.2, it is clear that the addition of another M atom into single atom catalyst (M_ZSM-5) to form dimer catalyst (M_2_ZSM-5) is energetically favorable. The energy gain is the most in case of Pt system when Pt_ZSM-5 is converted to Pt_2_ZSM-5.

Table 6.2: Energy gain with the addition of a gas phase M atom to the cluster (M=Au, Pd and Pt).

Species	E_{build} $(in\ kcal/mol)$
Au_2	-66.52
Pd_2	-27.72
Pt_2	-80.93

6.3.2 Adsorption of NO and O_2 on bare and ZSM-5 supported Au_n (n=1-2) system

The optimized geometries of bare and ZSM-5 supported single Au atom along with their NO and O_2 adsorbed structures are given in Figure 6.2. The bond lengths of O_2 and NO are found to be 1.205 Å and 1.153 Å, respectively, which corresponds closely with the values reported in the CRC Handbook of Chemistry and Physics [37]. The vibrational frequency of O_2 and NO are found to be 1734.44 cm^{-1} and 2048.19 cm^{-1} respectively, which are closer with the experimental values [38, 39]. In NO, Nitrogen has a positive charge of 0.115e while oxygen has a negative charge of -0.115e. While both the oxygen atoms in O_2 have a zero charge. The single monomeric Au is a neutral charge species with doublet as ground state spin multiplicity. The electronic configuration of single Au is $5d^{10}6s^1$ which means that 6s orbital is half filled. The spin states are {HOMO(α), LUMO(β)}. NO is adsorbed on bare monomeric Au in an end-on position [40] while O_2 is nominally adsorbed in a bridged manner. Table 6.3 includes adsorption energies (E_{ads}), bond parameters of NO/O_2 after adsorption and mulliken charges of adsorbed species. The adsorption energies of NO and O_2 on single Au atom are -8.82 kcal/mol and 0.41 kcal/mol, respectively (Table 6.3). Looking at the mulliken charges in Fig 1(b), it is evident that small amount of charge transfer has occurred from Au atom to NO. After adsorption, the bond length of NO has increased from 1.153 Å to 1.157 Å which indicates little activation of NO. However, when it comes to O_2, there is no favorable interaction between Au and O_2 (as indicated by the positive adsorption energy). The distance between Au and O_2 is also high (3.075 Å) and there is negligible or minimum charge transfer occurring between these two species. The bond length of adsorbed O_2 (1.205 Å) also indicates the same.

The ground state spin multiplicity of ZSM-5 supported single Au atom is doublet. The Mulliken charge of Au atom inside the support is -0.914e which

suggests that charge transfer has actually occurred from support to the monomeric Au atom. Owing to the substantial electronegativity, Au atoms/clusters readily withdraws electrons from supporting materials, resulting in a negative charge [41, 42]. The spin states are {HOMO(α), LUMO(β)}, same as bare system. This electron transfer from support to Au catalysts tend to improve interactions with the reactants. The adsorption energies of NO and O_2 on ZSM-5 supported monomeric Au atom are -16.14 kcal/mol and -3.09 kcal/mol, respectively (Table 6.3). Charge transfer has occurred from Au atom to NO as both N (-0.053e) and O (-0.143e) have acquired negative electronic charges. The main evidence was found from the bond length and vibrational frequency of NO. After adsorption, the bond length and vibrational frequency of NO are found to be 1.177 Å and 1760.49 cm^{-1}, which suggests activation of NO upon adsorption. Because of its π antibonding character in the nitrogen-oxygen bond, NO is a good π acceptor, meaning it may take electrons from a metal. When it comes to O_2 adsorption, the adsorption of O_2 on MFI supported monomeric Au have improved with respect to the unsupported bare Au atom. Mulliken charges suggests that minor charge transfer has taken place from O_2 molecule to Au (0.018e from each O atom of O_2). The strong electronegativity characteristics of gold (Au) facilitates charge transfer from oxygen molecule to gold. Comparatively, the charge transfer from O_2 to Au-ZSM-5 is greater than the charge transfer from O_2 to bare Au. This resulted in slight interaction between O_2 and Au in supported system; however, it doesn't activate O_2 much. Thus, the main conclusion is that support system has a positive impact on the adsorption and activation of the reactants for monomeric Au atom.

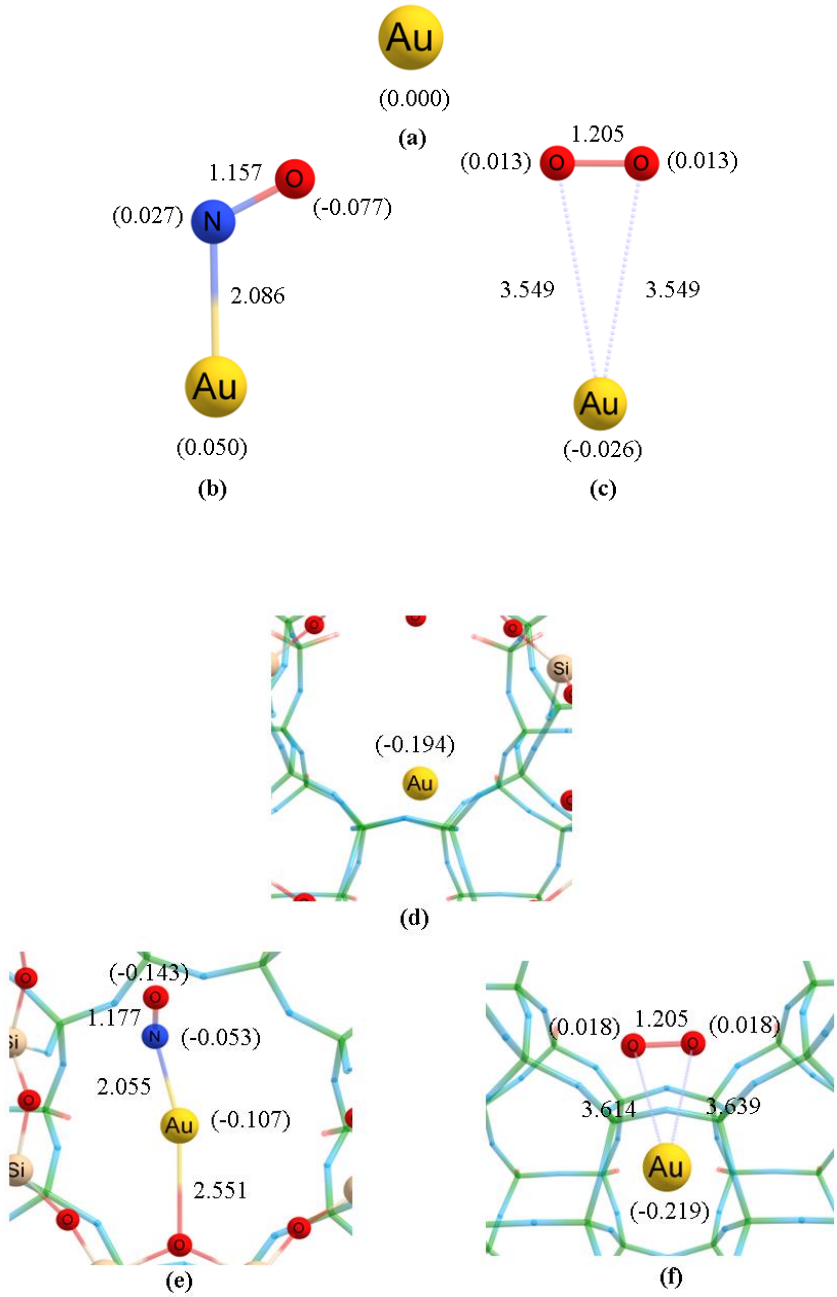

Figure 6.2: Optimized geometries of (a) bare Au (b) NO adsorbed on Au (c) O_2 adsorbed on Au (d) Au_MFI (e) NO adsorbed on Au_MFI and (f) O_2 adsorbed on Au_MFI. Bond lengths are included and mulliken charges are given in parentheses.

Au_2 dimer has a bond length of 2.557 Å and vibrational frequency of 172.86 cm^{-1}. The ground state spin multiplicity is singlet. The experimental values related to Au_2 dimer (d_{Au-Au}=2.472 Å and ν_{Au-Au}=191 cm^{-1}) justifies the basis set and functional used for this work [43]. The adsorption energies for NO and O_2 adsorption on bare Au_2 dimer are -10.17 kcal/mol and -1.81 kcal/mol, respectively.

However, looking at the bond parameters of adsorbed NO (d_{N-O}=1.150 Å and ν_{N-O}=2004.18 cm^{-1}), it is observed that NO is not at all activated which means minimum interaction is taking place between NO and Au_2 dimer. Mulliken charges on NO also indicating that little charge transfer has taken place from Au_2 dimer to NO. The same holds true for O_2, whose adsorption energy itself indicates that there is little interaction between Au_2 dimer and O_2. The bond length and vibrational frequency of O_2 after adsorption are 1.206 Å and 1704.56 cm^{-1}, respectively. Hence, it is clear that Au_2 dimer is unable to activate both the reactants. It may be due to the closed shell electronic configuration of Au_2 dimer. On the other hand, the adsorption energies for O_2 and NO on Au_2 dimer supported on MFI are determined to be 31.30 kcal/mol and -5.76 kcal/mol, respectively. By examining the bond characteristics of NO adsorbed on Au_2-ZSM-5 dimer (d_{N-O}=1.153 Å and ν_{N-O}=2023.05 cm^{-1}), it can be determined that NO is not activated at all. This suggests that the NO and Au_2 dimer inside ZSM-5 have very little interaction. The reason behind this could be that NO tends to bind in an end-on position with Au_2 dimers. But because of ZSM-5's confinement effect, it cannot adsorb in an end-on position, increasing the distance between NO and Au in the Au_2 dimer. The interaction between NO and Au is hindered by this increased distance, which is also reflected in their adsorption energy. Similar circumstances apply to O_2 adsorbed on Au_2-ZSM-5 dimer, where the confinement effect has a negative impact on the adsorption energy. Figure 6.3 shows optimized geometries of NO and O_2 adsorbed species on bare and ZSM-5 supported Au_2 dimer.

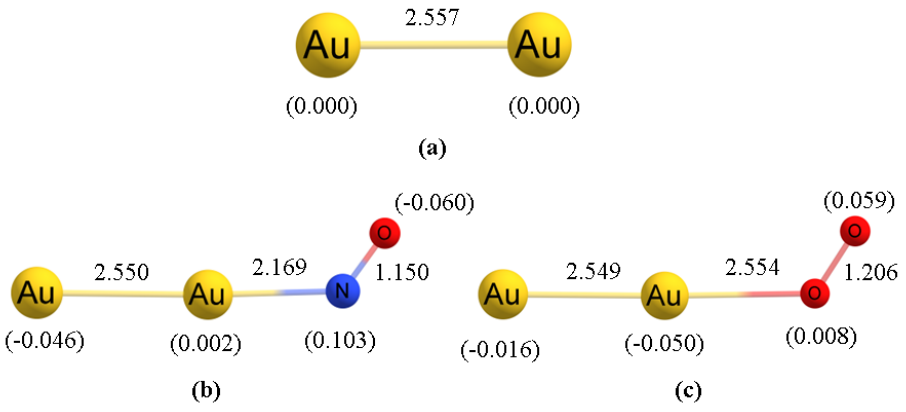

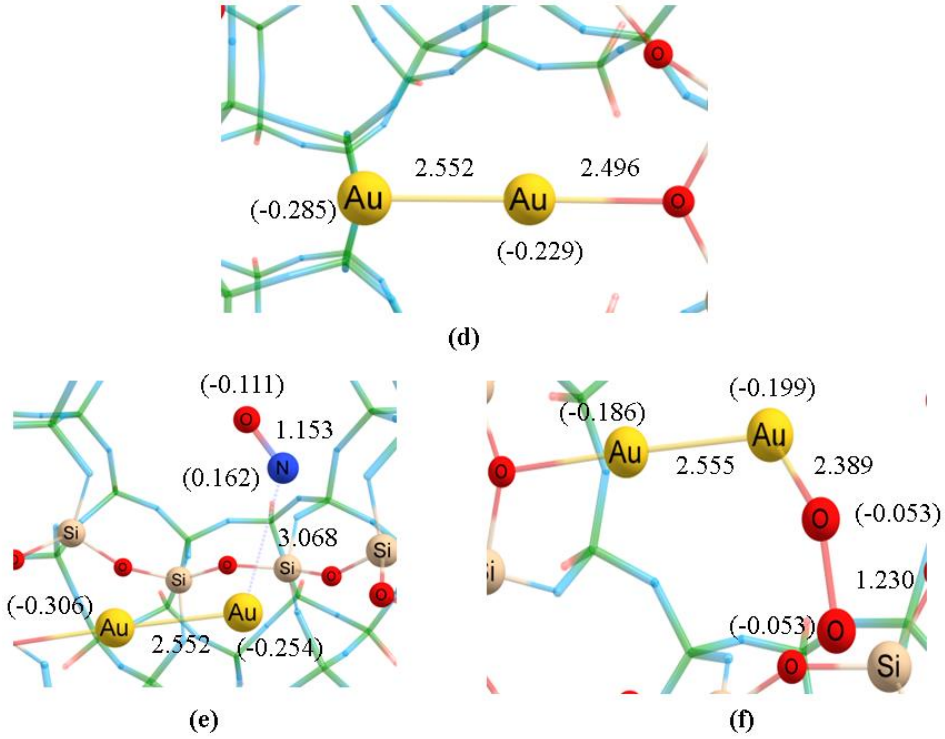

Figure 6.3: Optimized geometries of (a) bare Au_2 dimer (b) NO adsorbed on Au_2 dimer (c) O_2 adsorbed on Au_2 dimer (d) Au_2_MFI (e) NO adsorbed on Au_2_MFI and (f) O_2 adsorbed on Au_2_MFI. Bond lengths are included and mulliken charges are given in parentheses.

Table 6.3: Adsorption energies (E_{ads}), bond characteristics {bond lengths (d_{N-O}/d_{O-O}) and frequencies (ν_{N-O}/ν_{O-O})}, mulliken charge of Au (q_{Au}) in adsorbed configuration and mulliken charges of adsorbed NO and O_2 (q_{NO}/q_{O_2}). * indicates atom which is attached to the reactants (or catalysts).

Species	E_{ads} (in kcal/mol)	d_{N-O}/d_{O-O} (in Å)	ν_{N-O} / ν_{O-O} (in cm^{-1})	q_{Au}	q_{NO}/q_{O_2}
Au_NO	-8.82	1.157	1859.53	0.050	0.027(N*); -0.077(O)
Au_O_2	0.41	1.205	1727.39	-0.026	0.013(O*);

					0.013(O*)
Au_ZSM-5_NO	-16.14	1.177	1760.49	-0.107	-0.053(N*); -0.143(O)
Au_ZSM-5_O_2	-3.09	1.205	1733.22	-0.219	0.018(O*); 0.018(O*)
Au_2_NO	-10.17	1.150	2004.18	-0.046(Au) 0.002(Au*)	0.103(N*); -0.060(O)
Au_2_O_2	-1.81	1.206	1704.56	-0.016(Au) -0.050(Au*)	0.008(O*); 0.059(O)
Au_2_ZSM-5_NO	-5.76	1.153	2023.05	-0.306(Au) -0.254(Au*)	0.162(N*); -0.111(O)
Au_2_ZSM-5_O_2	31.30	1.230	1519.39	-0.186(Au) -0.199(Au*)	-0.053(O*); -0.053(O)

6.3.3 Adsorption of NO and O_2 on bare and ZSM-5 supported Pd_n (n=1-2) system

Pd monomer is a neutral species with $4d^{10}$ electronic configuration and ground state multiplicity of singlet. NO is adsorbed on Pd atom in an end-on configuration. While doing so, the bond length of NO elongates upto 1.168 Å and the vibrational frequency decreases to 1884.22 cm^{-1} (redshift occurs). Mulliken charge analysis shows that Pd atom has become more positive (0.107e) which suggests charge transfer from Pd to π* orbitals of NO. Charge transfer from Pd filled *d* orbitals to antibonding NO orbitals leads to the activation of NO. The E_{ads} of NO on Pd monomer is calculated to be -23.30 kcal/mol. The adsorption pattern and energies of NO adsorbed on single Pd atom found in our study is similar to previously reported results [44]. O_2 is also adsorbed in an end-on position. When O_2 is adsorbed on Pd monomer, its vibrational frequency decreases from 1734.43 cm^{-1} (free O_2) to 1430.52 cm^{-1}. The bond length of O_2 increases from 1.205 Å to 1.251 Å.

Both the parameters suggest activation of O_2 upon adsorption on single Pd atom. More positive charge on Pd atom (0.213e) and negative charges on O_2 (-0.134e and -0.080e) also indicates charge transfer from Pd to π* orbitals of O_2. The E_{ads} of O_2 adsorbed on Pd atom is -11.07 kcal/mol.

The negative charge (-0.198e) of the Pd monomer inside the ZSM-5 indicates that charge transfer from the support to the Pd atom has likely taken place. The adsorption pattern of both the reactants is same as that of bare Pd atom. However, E_{ads} of NO and O_2 adsorbed on MFI supported Pd atom are -33.10 kcal/mol and -21.49 kcal/mol, respectively. It is to be noted that the E_{ads} of NO and O_2 on MFI supported Pd are larger than that of bare Pd monomer. Moreover, NO is much more activated in support system (d_{N-O}=1.174 Å and ν_{N-O}=1846.80 cm^{-1}). Same is the case for O_2 (d_{O-O}=1.265 Å and ν_{O-O}=1356.48 cm^{-1}) where it is much more activated in support in comparison to the bare single Pd atom. It may be attributed to the fact that Pd atom inside the zeolite pore has a negative charge (-0.198e). Hence, it becomes easier for Pd to transfer electrons to the antibonding orbitals of NO and O_2, which results in the activation of both the reactants. Hence, confinement effect has a positive influence on the adsorption and activation of NO and O_2 over Pd monomer. Figure 6.4 includes adsorbed configurations of NO and O_2 on bare and ZSM-5 supported Pd monomer.

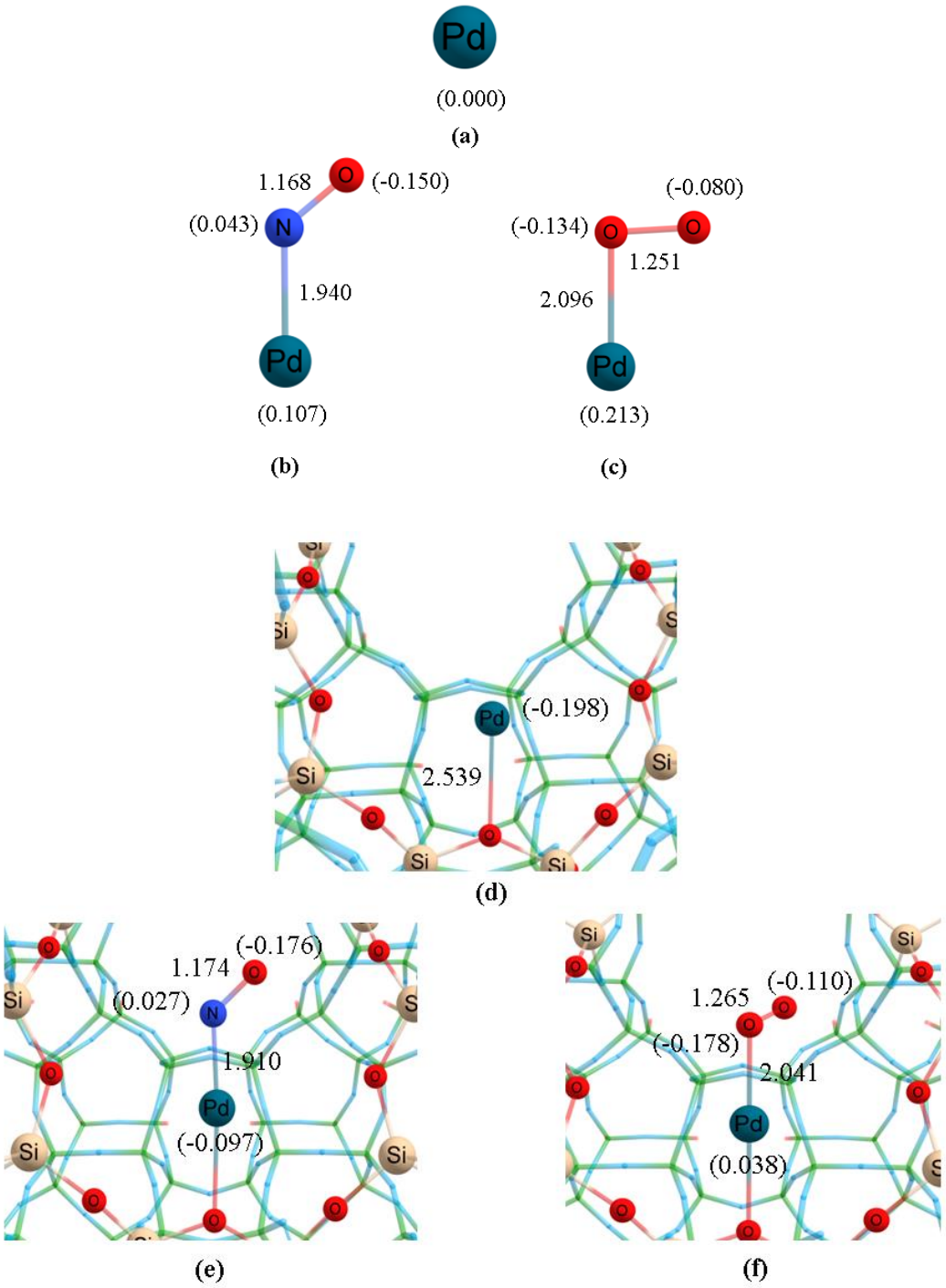

Figure 6.4: Optimized geometries of (a) bare Pd (b) NO adsorbed on Pd (c) O_2 adsorbed on Pd (d) Pd_MFI (e) NO adsorbed on Pd_MFI and (f) O_2 adsorbed on Pd_MFI. Bond lengths are included and mulliken charges are given in parentheses.

Figure 6.5 includes adsorbed NO and O_2 structures on bare and ZSM-5 supported Pd_2 dimer. Pd_2 dimer has a bond length of 2.790 Å with ground state spin multiplicity of singlet. Each Pd atom has an electronic configuration of $5s^{0.04}4d^{9.95}$.

The E_{ads} of NO and O_2 adsorbed on Pd_2 dimer are found to be -43.42 kcal/mol and -27.25 kcal/mol, respectively. NO is adsorbed in a bridged end-on configuration manner where N atom of NO is linked to both the Pd atoms. This resulted in red shift of frequency {from 2048.19 cm^{-1} (free NO) to 1707.34 cm^{-1}}. The positive electronic charges on both the Pd atoms (0.146e) reveals equal charge transfer from both the Pd atoms to the π* orbitals of NO. O_2 is adsorbed on Pd_2 dimer in a bridge side-on two site configuration where each O is attached to its nearby Pd atom. This configuration leads to elongation and activation of O_2 which is evident from its bond length (1.286 Å) and frequency (1287.80 cm^{-1}). Each O atom of O_2 is receiving 0.174e from its nearby Pd atom. It is to note that the E_{ads} and activation of NO and O_2 is much more in case of Pd_2 dimer than that of Pd monomer. It is also evident that Pd_2 dimer is able to transfer more charge into the antibonding orbitals of NO and O_2 which ultimately resulted in their activation. When it comes to support system, the bond length and vibrational frequency of Pd_2 inside ZSM-5 are 2.749 Å and 123.44 cm^{-1}, respectively. As similar to Au_2, Pd_2 also acquire negative charge which suggests charge transfer from support to the catalyst. The adsorption configuration of NO and O_2 in MFI supported Pd_2 dimer is exactly similar to that of bare Pd_2 dimer. However, the value of E_{ads} (given in Table 6.4) indicates that the adsorption energies have increased in ZSM-5 supported Pd_2. The E_{ads} of NO and O_2 on Pd_2-ZSM- 5 have increased upto approx. 6 kcal/mol and 10 kcal/mol, respectively in comparison to the bare counterpart. Looking at the bond parameters of NO adsorbed on Pd_2-ZSM- 5 (d_{N-O}=1.203 Å and ν_{N-O}=1673.03 cm^{-1}), it is evident that NO is sufficiently activated. The bond parameters of O_2 (d_{O-O}=1.293 Å and ν_{O-O}=1270.40 cm^{-1}) adsorbed on Pd_2-ZSM-5 also indicates activation of O_2. It is evident that ZSM-5 positively affects the reactants' activation and adsorption on Pd monomer as well as dimer. Table 6.4 includes adsorption energies (E_{ads}), bond parameters of NO/O_2 after adsorption and mulliken charges of adsorbed species on bare and supported Pd monomer and dimer.

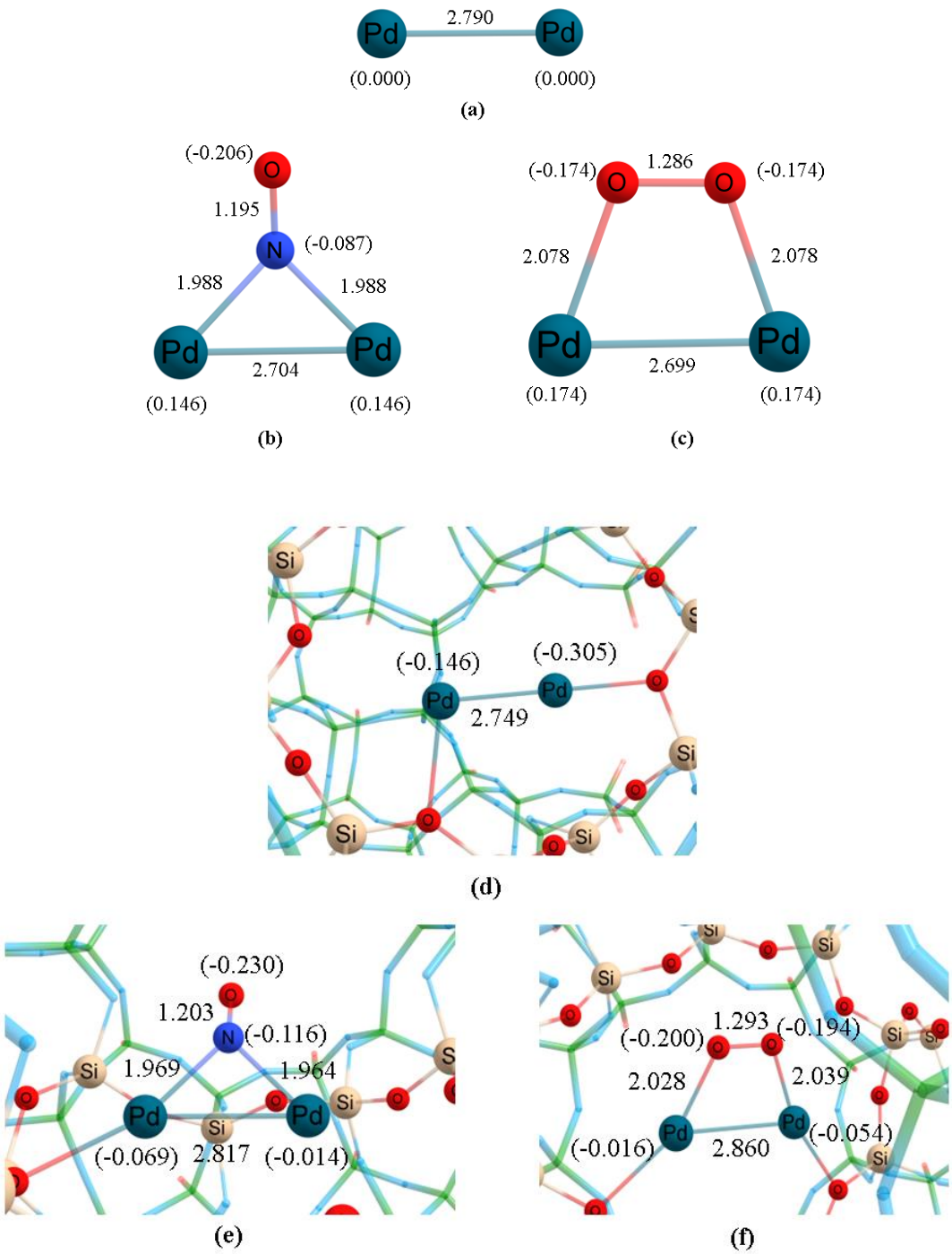

Figure 6.5: Optimized geometries of (a) bare Pd_2 dimer (b) NO adsorbed on Pd_2 dimer (c) O_2 adsorbed on Pd_2 dimer (d) Pd_2_MFI (e) NO adsorbed on Pd_2_MFI and (f) O_2 adsorbed on Pd_2_MFI. Bond lengths are shown and mulliken charges are given in parentheses.

Table 6.4: Adsorption energies (E_{ads}), bond characteristics {bond lengths (d_{N-O}/d_{O-O}) and frequencies (ν_{N-O}/ν_{O-O})}, mulliken charge of Pd (q_{Pd}) in

adsorbed configuration and mulliken charges of adsorbed NO and O_2 (q_{NO}/q_{O_2}). * indicates atom which is attached to the reactants (or catalysts).

Species	E_{ads} (in kcal/mol)	d_{N-O}/d_{O-O} (in Å)	ν_{N-O} / ν_{O-O} (in cm^{-1})	q_{Pd}	q_{NO}/q_{O_2}
Pd_NO	-23.30	1884.22	1.168	0.107	0.043(N*); -0.150(O)
Pd_ZSM-5_NO	-33.10	1846.80	1.174	-0.097	0.027(N*) -0.176(O)
Pd_O_2	-11.07	1430.52	1.251	0.213	-0.134(O*) -0.080(O)
Pd_ZSM-5_O_2	-21.49	1356.48	1.265	0.038	-0.178(O) -0.110(O)
Pd_2_NO	-43.42	1707.34	1.195	0.146(Pd*) 0.146(Pd*)	-0.087(N*) -0.260(O)
Pd_2_ZSM-5_NO	-49.48	1673.03	1.203	-0.069(Pd*) -0.014(Pd*)	-0.116(N*) -0.230(O)
Pd_2_O_2	-27.25	1287.80	1.286	0.174(Pd*) 0.174(Pd*)	-0.174(O*) -0.174(O*)
Pd_2_ZSM-5_O_2	-37.46	1270.40	1.293	-0.016(Pd*) -0.054(Pd*)	-0.200(O*) -0.194(O*)

6.3.4 Adsorption of NO and O_2 on bare and ZSM-5 supported Pt_n (n=1-2) system

Pt monomer has a $6s^15d^9$ configuration with ground state spin multiplicity of triplet. The spin states are {HOMO(α), LUMO(β)} for the bare system. Both NO and O_2 gets adsorbed to Pt atom in an end-on configuration. Structures of NO and O_2

adsorbed species on Pt atom is given in Figure 6.6. Upon adsorption, the bond length of N-O bond gets elongated upto 1.168 Å. Moreover, redshift in frequency occurs (1860.25 cm^{-1}). Total 0.173e charge is transferred from Pt to NO which resulted in the activation of NO. Negative charges on N atom (-0.027e) and O atom (-0.145e) shows direction of electron movement from metal to NO. Similar is the scenario for O_2 where the bond parameters also suggest activation of O_2. Upon adsorption, the bond length of O_2 increases to 1.258 Å and frequency decreases to 1372.84 cm^{-1}. Total of 0.249e charge gets transferred from filled Pt orbitals to antibonding orbitals of O_2. The E_{ads} of NO and O_2 on bare Pt monomer are -53.64 kcal/mol and -22.72 kcal/mol, respectively. It is noteworthy that the adsorption energies are larger, indicating a greater amount of interaction between the reactants and Pt's 5d orbitals. Regarding the Pt monomer supported by MFI, the charge on the free Pt atom (-0.276e) indicates a possible transfer of charge from the support to the Pt atom. Table 6.5 includes adsorption energies (E_{ads}), bond parameters of NO/O_2 after adsorption and mulliken charges of adsorbed species on bare and supported Pt monomer and dimer. The adsorption pattern of NO and O_2 on MFI supported single Pt atom is also same as that of bare monomeric system. However, looking at Figure 6.6 and Table 6.5, it is obvious that the activation is much more in case of the support system. The bond parameters of NO and O_2 adsorbed on MFI supported Pt atom also indicates the same. This suggest that the charge transfer from Pt atom to the reactants is much more in case of support system than that of bare system. The E_{ads} of NO and O_2 on ZSM-5 supported Pt atom have increased with respect to the bare Pt monomer system, which indicates positive influence of the support. The E_{ads} of NO and O_2 on ZSM-5 supported single Pt atom are found to be -61.21 kcal/mol and -34.13 kcal/mol, respectively. The E_{ads} of NO on the support system is 7.57 kcal/mol higher than the bare Pt atom while E_{ads} of O_2 on the support system is 11.41 kcal/mol higher.

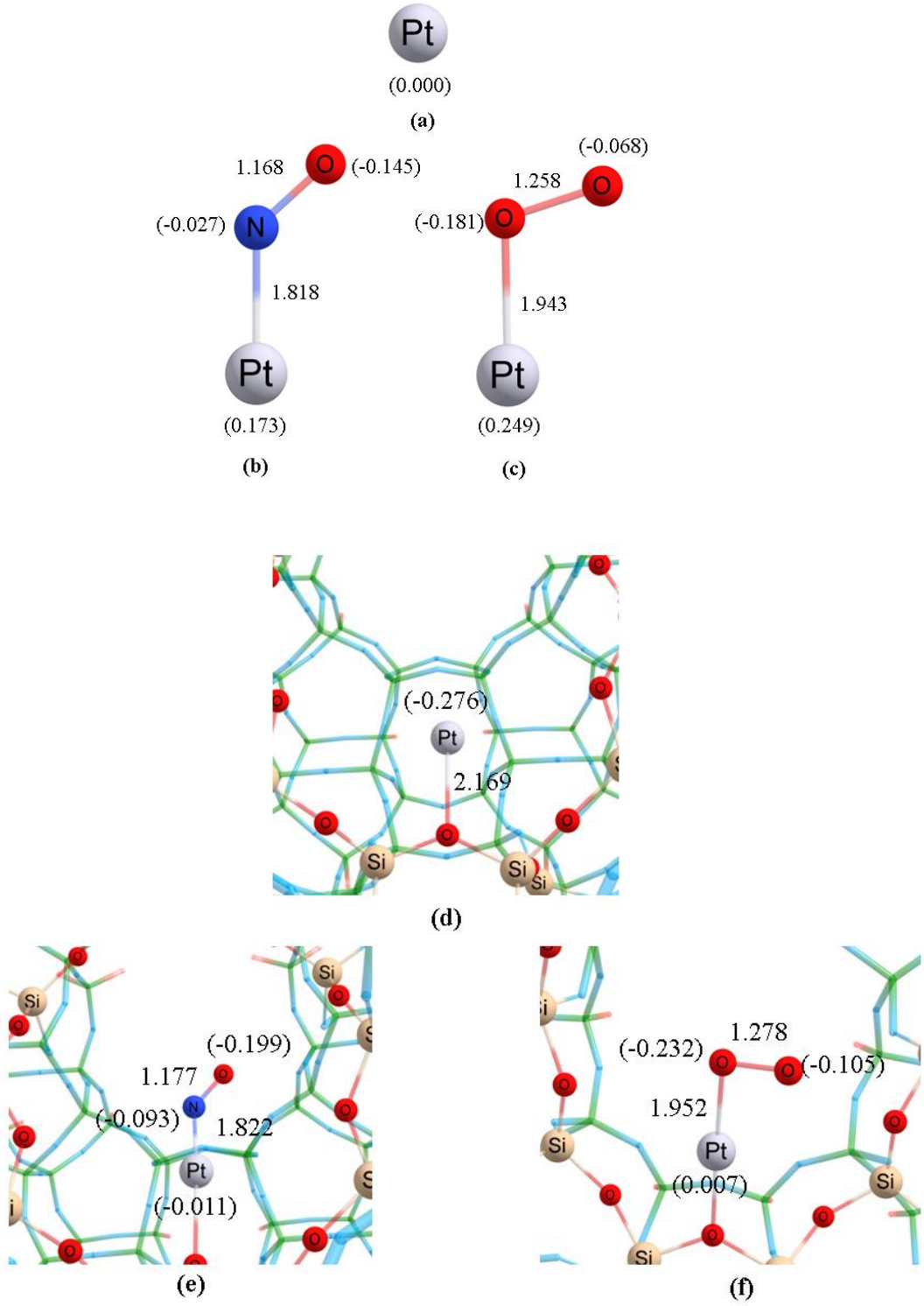

Figure 6.6: Optimized geometries of (a) bare Pt (b) NO adsorbed on Pt (c) O_2 adsorbed on Pt (d) Pt_MFI (e) NO adsorbed on Pt_MFI and (f) O_2 adsorbed on Pt_MFI. Bond lengths are shown and mulliken charges are given in parentheses.

Pt_2 dimer is a neutral species with each Pt atom having electronic configuration of $6s^{0.69}5d^{9.29}$. The spin states for the bare dimer systems are

{HOMO(β), LUMO(β)}. NO is adsorbed to one of the Pt atoms of Pt_2 dimer in an end-on configuration with E_{ads} of -76.86 kcal/mol. However, the bond length of adsorbed NO (1.148 Å) and frequency (2017.45 cm^{-1}) suggest minimum activation of NO upon adsorption on Pt_2 dimer. O_2 is adsorbed in bridge side-on two site configuration where each O is attached to its nearby Pt atom. From each Pt atom, 0.325e is transferred to the nearby O atom of O_2. The bond length of adsorbed O_2 (1.409 Å) and vibrational frequency (893.62 cm^{-1}) suggest that O_2 gets highly activated upon adsorption on Pt_2 dimer. The E_{ads} of O_2 adsorbed on bare Pt_2 dimer is found to be -39.46 kcal/mol. When it comes to support system, the E_{ads} of both NO and O_2 decreases. The spin states for the supported dimer systems are {HOMO(β), LUMO(β)}. The adsorption pattern is also same as that of bare system. Upon adsorption on Pt_2-ZSM-5, NO is much more activated in comparison to bare Pt_2 system. However, E_{ads} of NO is lower in the support system. For O_2, looking at the bond parameters (d_{O-O}=1.322 Å and ν_{O-O}=1143.31 cm^{-1}), it is evident that activation of O_2 on Pt_2-ZSM-5 is lower in comparison to bare Pt_2 dimer. The adsorbed configurations of NO and O_2 on bare and ZSM-5 supported Pt_2 dimer are given in Figure 6.7.

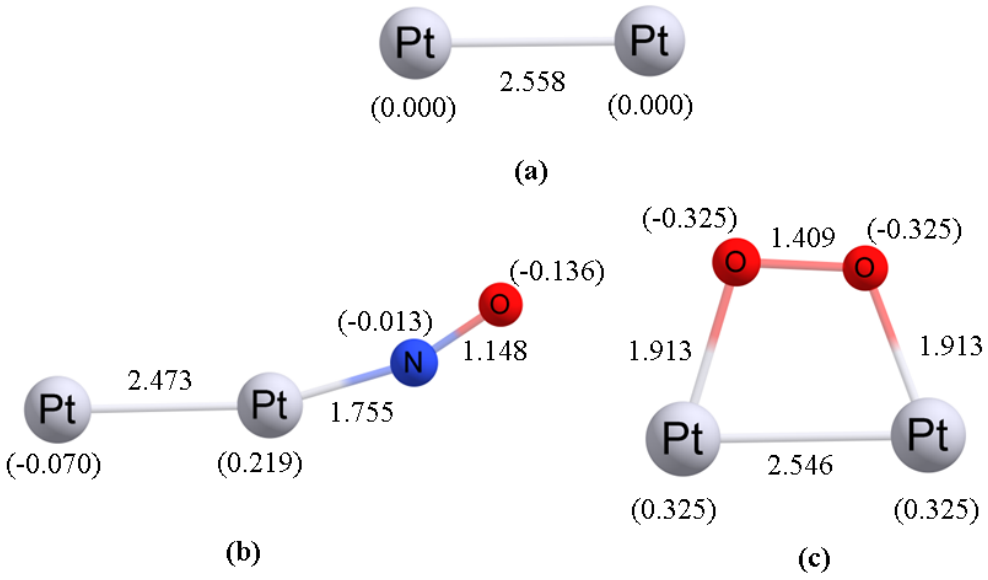

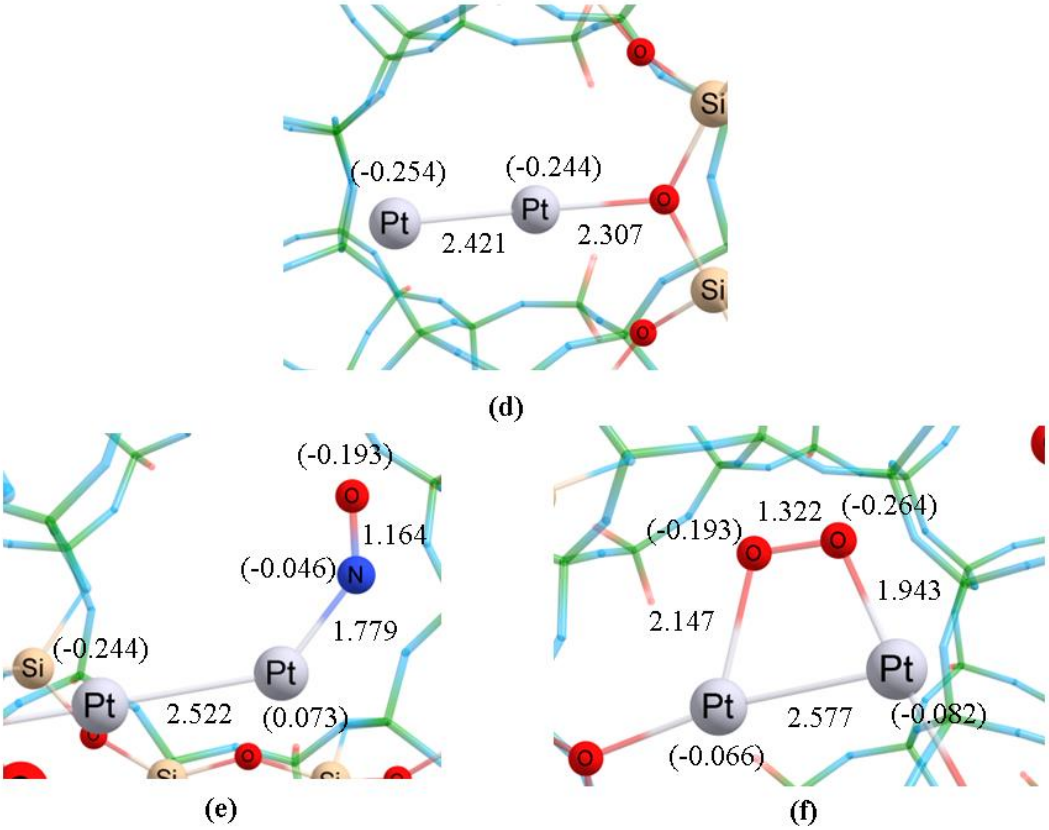

Figure 6.7: Optimized geometries of (a) bare Pt_2 dimer (b) NO adsorbed on Pt_2 dimer (c) O_2 adsorbed on Pt_2 dimer (d) Pt_2_MFI (e) NO adsorbed on Pt_2_MFI and (f) O_2 adsorbed on Pt_2_MFI. Bond lengths are shown and mulliken charges are given in parentheses.

Table 6.5: Adsorption energies (E_{ads}), bond characteristics {bond lengths (d_{N-O}/d_{O-O}) and frequencies (ν_{N-O}/ν_{O-O})}, mulliken charge of Pd (q_{Pt}) in adsorbed configuration and mulliken charges of adsorbed NO and O_2 (q_{NO}/q_{O_2}). * indicates atom which is attached to the reactants (or catalysts).

Species	E_{ads}(in kcal/mol)	d_{N-O}/d_{O-O} (in Å)	ν_{N-O} / ν_{O-O} (in cm^{-1})	q_{Pt}	q_{NO}/q_{O_2}
Pt_NO	-53.64	1860.25	1.168	0.173	-0.027(N*); -0.145(O)
Pt_ZSM-5_NO	-61.21	1835.19	1.177	-0.011	-0.093(N*)

					-0.199(O)
Pt_O_2	-22.72	1372.84	1.258	0.249	-0.181(O*) -0.068(O)
$Pt\_ZSM\text{-}5\_O_2$	-34.13	1319.39	1.278	0.007	-0.232(O*) -0.105(O)
Pt_2_NO	-76.86	2017.45	1.148	0.219(Pt*) -0.070(Pt)	-0.013(N*) -0.136(O)
$Pt_2\_ZSM\text{-}5\_NO$	-40.50	1888.28	1.164	0.073(Pt*) -0.244(Pt)	-0.046(N*) -0.193(O)
$Pt_2\_O_2$	-39.46	893.62	1.409	0.325(Pt*) 0.325(Pt*)	-0.325(O*) -0.325(O*)
$Pt_2\_ZSM\text{-}5\_O_2$	-26.98	1143.31	1.322	-0.066(Pt*) -0.082(Pt*)	-0.193(O*) -0.264(O*)

6.4 Significant Outcomes

In this work, we have used DFT based ONIOM method to investigate the adherence of the M_n system (M=Au, Pd and Pt) (n=1-2) to the main channel of a purely siliceous ZSM-5 zeolite.

1. We have found that the binding energy of single atom on ZSM-5 framework is energetically unfavorable; however, the formation of dimer system onto the support is energetically feasible.
2. Our analysis of the structures of the supported monomers and dimers shows that the interaction with the support causes notable modifications to the geometric and electronic properties of the clusters as well as deformation to the framework. The adsorption energy of NO and O_2 can be significantly influenced by the metal-support interaction.

3. The results show that adsorption energies of NO and O_2 on ZSM-5 supported single metal atom is more in comparison to that of bare single metal atom.
4. Mulliken charge analysis indicates that substantial amount of charge transfer takes place from support to the metal which aids metal to donate electrons to the antibonding orbitals of NO and O_2.
5. However, when it comes to dimer system inside ZSM-5, Au_2 and Pt_2 have lower adsorption energies with respect to the bare dimer system. For Pd_2 dimer, the support has a positive influence on the adsorption energies.
6. Compared to NO and O_2 adsorbed on a free cluster, the cluster-support interaction typically causes more redshift on the NO and O_2 stretching modes.

6.5 Bibliography

[1] Monks, P. S. Gas-phase radical chemistry in the troposphere. *Chemical Society Reviews*, 34:376-395, 2005.

[2] Tsukahara, H., Ishida, T., and Mayumi, M. Gas-phase oxidation of nitric oxide: chemical kinetics and rate constant. *Nitric Oxide*, 3:191-198, 1999.

[3] Mulla, S. S., Chen, N., Cumaranatunge, L., Blau, G. E., Zemlyanov, D. Y., Delgass, W. N., Epling, W. S., and Ribeiro, F. H. Reaction of NO and O_2 to NO_2 on Pt: Kinetics and catalyst deactivation. *Journal of Catalysis*, 241:389-399, 2006.

[4] Wang, Z., Lin, F., Jiang, S., Qiu, K., Kuang, M., Whiddon, R., and Cen, K. Ceria substrate–oxide composites as catalyst for highly efficient catalytic oxidation of NO by O_2. *Fuel*, 166:352-360, 2016.

[5] Wang, H. F., Guo, Y. L., Lu, G., and Hu, P. NO oxidation on platinum group metals oxides: first principles calculations combined with microkinetic analysis. *The Journal of Physical Chemistry C*, 113:18746-18752, 2009.

[6] Zhang, J., Wang, L., Zhang, B., Zhao, H., Kolb, U., Zhu, Y., Liu, L., Han, Y., Wang, G., Wang, C., and Su, D. S. Sinter-resistant metal nanoparticle catalysts achieved by immobilization within zeolite crystals via seed-directed growth. *Nature Catalysis*, 1:540-546, 2018.

[7] Moliner, M., Gabay, J., Kliewer, C., Serna, P., and Corma, A. Trapping of metal atoms and metal clusters by chabazite under severe redox stress. *ACS Catalysis*, 8:9520-9528, 2018.

[8] Wang, N., Sun, Q. and Yu, J. Ultrasmall metal nanoparticles confined within crystalline nanoporous materials: a fascinating class of nanocatalysts. *Advanced Materials*, 31:1803966, 2019.

[9] Wu, S.M., Yang, X.Y. and Janiak, C. Confinement effects in zeolite-confined noble metals. *Angewandte Chemie*, 131:12468-12482, 2019.

[10] Busca, G., Lietti, L., Ramis, G., and Berti, F. Chemical and mechanistic aspects of the selective catalytic reduction of NO_x by ammonia over oxide catalysts: a review. *Applied Catalysis B: Environmental*, 18:1-36, 1998.

[11] Centi, G. and Perathoner, S. Nature of active species in copper-based catalysts and their chemistry of transformation of nitrogen oxides. *Applied Catalysis A: General*, 132:179-259, 1995.

[12] Nova, I. and Tronconi, E. Urea-SCR technology for deNOx after treatment of diesel exhausts. Springer New York, 2014.

[13] Beale, A. M., Gao, F., Lezcano-Gonzalez, I., Peden, C. H., and Szanyi, J. Recent advances in automotive catalysis for NO_x emission control by small-pore microporous materials. *Chemical Society Reviews*, 44:7371-7405, 2015.

[14] Granger, P. and Parvulescu, V. I. Catalytic NO_x abatement systems for mobile sources: from three-way to lean burn after-treatment technologies. *Chemical Reviews*, 111:3155-3207, 2011.

[15] Ennaert, T., Van Aelst, J., Dijkmans, J., De Clercq, R., Schutyser, W., Dusselier, M., Verboekend, D., and Sels, B. F. Potential and challenges of zeolite chemistry in the catalytic conversion of biomass. *Chemical Society Reviews*, 45:584-611, 2016.

[16] Schwach, P., Pan, X., and Bao, X. Direct conversion of methane to value-added chemicals over heterogeneous catalysts: challenges and prospects. *Chemical reviews*, 117:8497-8520, 2017.

[17] Ilias, S. and Bhan, A. Mechanism of the catalytic conversion of methanol to hydrocarbons. Acs Catalysis, 3:18-31, 2013.

[18] Gu, Y., Majumdar, S. S., Pihl, J. A., and Epling, W. S. Investigation of NO adsorption and desorption phenomena on a Pd/ZSM-5 passive NO_x adsorber. *Applied Catalysis B: Environmental*, 298:120561, 2021.

[19] Hamid, Y., Matarrese, R., Morandi, S., Castoldi, L., and Lietti, L. Pd-Doped SSZ-13 for Low-T NO_x Adsorption: an Operando FT-IR Spectroscopy Study. *Topics in Catalysis*, 66:750-760, 2023.

[20] Grybos, R., Benco, L., Bučko, T., and Hafner, J. Molecular adsorption and metal-support interaction for transition-metal clusters in zeolites: NO adsorption on Pd_n (n= 1–6) clusters in mordenite. *The Journal of chemical physics*, 130:104503, 2009.

[21] Sierraalta, A., Alejos, P., and Ehrmann, E. Influence of isomorphous substitution on NO and N_2O thermochemistry on Au/ZSM-5 catalyst. *International Journal of Quantum Chemistry*, 108:1696-1704, 2008.

[22] Sobczak, I., Musialska, K., Pawlowski, H., and Ziolek, M. NO and C_3H_6 adsorption and coadsorption in oxygen excess—A comparative study of different type zeolites modified with gold. *Catalysis today*, 176:393-398, 2011.

[23] Xie, C., Niu, Z., Kim, D., Li, M., and Yang, P. Surface and interface control in nanoparticle catalysis. *Chemical reviews*, 120:1184-1249, 2019.

[24] Maseras, F. and Morokuma, K. IMOMM: A new integrated ab initio+ molecular mechanics geometry optimization scheme of equilibrium structures and transition states. *Journal of Computational Chemistry*, 16:1170-1179, 1995.

[25] Chung, L. W., Sameera, W. M. C., Ramozzi, R., Page, A. J., Hatanaka, M., Petrova, G. P., Harris, T. V., Li, X., Ke, Z., Liu, F., and Li, H. B. The ONIOM method and its applications. *Chemical reviews*, 115:5678-5796, 2015.

[26] Frisch, M. J.; Trucks, G. W.; Schlegel, H. B.; Scuseria, G. E.; Robb, M. A.; Cheeseman, J. R.; Scalmani, G.; Barone, V.; Mennucci, B.; Petersson, G. A.; *et al.Gaussian09*,Revision D.01, Gaussian, Inc.: Wallingford CT. 2010.

[27] Sillar, K. and Burk, P. Hybrid quantum chemical and density functional theory (ONIOM) study of the acid sites in zeolite ZSM-5. *The Journal of Physical Chemistry B*, 108:9893-9899, 2004.

[28] Patet, R. E., Caratzoulas, S., and Vlachos, D. G. Adsorption in zeolites using mechanically embedded ONIOM clusters. *Physical Chemistry Chemical Physics*, 18:26094-26106, 2016.

[29] Pantu, P., Boekfa, B., and Limtrakul, J. The adsorption of saturated and unsaturated hydrocarbons on nanostructured zeolites (H-MOR and H-FAU): An ONIOM study. *Journal of Molecular Catalysis A: Chemical*, 277:171-179, 2007.

[30] Chai, J. D. and Head-Gordon, M. Long-range corrected hybrid density functionals with damped atom–atom dispersion corrections. *Physical Chemistry Chemical Physics*, 10:6615-6620, 2008.

[31] Javadian, S. and Ektefa, F. An efficient approach to explore the adsorption of benzene and phenol on nanostructured catalysts: a DFT analysis. *RSC advances*, 5:100799-100808, 2015.

[32] Li, S., Zhao, Z., Zhao, R., Zhou, D., and Zhang, W. Aluminum location and acid strength in an aluminum-rich Beta zeolite catalyst: a combined density functional theory and solid-state NMR study. *ChemCatChem*, 9:1494-1502, 2017.

[33] Fellah, M. F. Adsorption of hydrogen sulfide as initial step of H_2S removal: A DFT study on metal exchanged ZSM-12 clusters. *Fuel Processing Technology*, 144:191-196, 2016.

[34] Bertin, V., Cruz, A., Del Angel, G., Castro, M., and Poulain, E. The H and H_2 interaction with Pd_3Cu, Pd_4, and Cu_4 fcc (111) clusters: A DFT comparative study. *International journal of quantum chemistry*, 102:1092-1105, 2005.

[35] Limtrakul, J., Nanok, T., Jungsuttiwong, S., Khongpracha, P., and Truong, T. N. Adsorption of unsaturated hydrocarbons on zeolites: the effects of the zeolite framework on adsorption properties of ethylene. *Chemical physics letters*, 349:161-166, 2001.

[36] Foster, J. P. and Weinhold, F. Natural hybrid orbitals. *Journal of the American Chemical Society*, 102:7211-7218, 1980.

[37] Lide D. R. *CRC handbook of chemistry and physics*, CRC Press, New York, 89th edition, 2009.

[38] Khanal, G. P., Parajuli, R., Arunan, E., Yamabe, S., Hiraoka, K., and Torikai, E. Study of structures, energies and vibrational frequencies of $(O_2)_n^+$ (n= 2–5) clusters by GGA and meta-GGA density functional methods. *Computational and Theoretical Chemistry*, 1056:24-36, 2015.

[39] Irikura, K. K. Experimental vibrational zero-point energies: Diatomic molecules. *Journal of physical and chemical reference data*, 36:389-397, 2007.

[40] Kuang, X. J., Wang, X. Q., and Liu, G. B. All-electron scalar relativistic calculation on the interaction between nitric monoxide and small gold cluster. *The European Physical Journal D*, 61:71-80, 2011.

[41] Sun, Q., Jena, P., Kim, Y. D., Fischer, M., and Ganteför, G. Interactions of Au cluster anions with oxygen. *The Journal of chemical physics*, 120:6510-6515, 2004.

[42] Sanchez, A., Abbet, S., Heiz, U., Schneider, W. D., Häkkinen, H., Barnett, R. N., and Landman, U. When gold is not noble: nanoscale gold catalysts. *The Journal of Physical Chemistry A*, 103:9573-9578, 1999.

[43] Varganov, S. A., Olson, R. M., Gordon, M. S., and Metiu, H. The interaction of oxygen with small gold clusters. *The Journal of chemical physics*, 119:2531-2537, 2003.

[44] Lacaze-Dufaure, C., Roques, J., Mijoule, C., Sicilia, E., Russo, N., Alexiev, V., and Mineva, T. A DFT study of the NO adsorption on Pd_n (n= 1–4) clusters. *Journal of Molecular Catalysis A: Chemical*, 341:28-34, 2011.